Proceedings of the ASME 2017 Smart Materials, Adaptive Structures and Intelligent Systems
SMASIS2017
September 18-20, 2017, Snowbird, UT, USA

SMASIS2017-3856

INTERNAL POROSITY DETECTION IN ADDITIVELY MANUFACTURED PARTS VIA ELECTROMECHANICAL IMPEDANCE MEASUREMENTS

Charles Tenney[1] **Mohammad I. Albakri**[1,*] **Joseph Kubalak**[2]
Logan D. Sturm[2] **Christopher B. Williams**[2] **Pablo A. Tarazaga**[1]

[1]Vibrations, Adaptive Structures, and Testing Laboratory
[2]Design, Research, and Education for Additive Manufacturing Systems Laboratory
Department of Mechanical Engineering, Virginia Tech
Blacksburg, VA, USA

ABSTRACT

The flexibility offered by additive manufacturing (AM) technologies to fabricate complex geometries poses several challenges to non-destructive evaluation (NDE) and quality control (QC) techniques. Existing NDE and QC techniques are not optimized for AM processes, materials, or parts. Such lack of reliable means to verify and qualify AM parts is a significant barrier to further industrial adoption of AM technologies.

Electromechanical impedance measurements have been recently introduced as an alternative solution to detect anomalies in AM parts. With this approach, piezoelectric wafers bonded to the part under test are utilized as collocated sensors and actuators. Due to the coupled electromechanical characteristics of piezoelectric materials, the measured electrical impedance of the piezoelectric wafer depends on the mechanical impedance of the part under test, allowing build defects to be detected. This paper investigates the effectiveness of impedance-based NDE approach to detect internal porosity in AM parts. This type of build defects is uniquely challenging as voids are normally embedded within the structure and filled with unhardened model or supporting material. The impact of internal voids on the electromechanical impedance of AM parts is studied at several frequency ranges.

Keywords: Electromechanical impedance, nondestructive evaluation, additive manufacturing, internal porosity.

*Address all correspondence to this author. Email: malbakri@vt.edu

INTRODUCTION

Additive manufacturing (AM) enables designers to realize products featuring complex geometries. AM products can be tailored to meet several design objectives and functionalities. The unique capabilities and flexibility of AM technologies have lead to a significant increase in the number of end-use products fabricated via AM. With such wide adoption of AM products comes the need for developing new non-destructive evaluation (NDE) and quality control (QC) techniques that can handle the complexity of such products.

Current NDE and QC techniques are not ideal for the inspection of complex AM products. NDE techniques based on dimensional measurement require access to all surfaces of the part, which is not always possible. The limited surface penetration of Ultrasonic-based NDE techniques, along with their sensitivity to surface roughness, restrict their applicability. Computed tomography has proven to be capable of inspecting the entirety of the part to detect deeply embedded defects. However, this technique is costly, time-consuming, and unable to detect cracks oriented perpendicular to the x-ray beam [1], [2].

In previous research efforts, the authors proposed the use of electromechanical impedance measurements as a means for NDE of AM parts [3]–[5]. Electromechanical impedance measurements use piezoelectric materials to interrogate the part under test at a given frequency range. With this approach, the functionality of the AM part is tested by measuring its dynamic response. In these studies, it has been demonstrated that electromechanical impedance NDE is capable of detecting parts

with dimensional inaccuracies, positional inaccuracies, and internal porosities.

This work further investigates the effectiveness of impedance-based NDE approach to AM defects, with the focus being turned towards internal porosity build errors. Such build errors would be expected from malicious attacks altering part files, since they can change the strength of the final product without significantly changing its mass [6]. The fact that internal voids can be filled with support material further minimizes changes in the total mass of the part, making the detection of such build errors even more challenging. For this purpose, a suite of simple test specimens has been designed featuring this build error. Voids are introduced to the parts at several locations so as to aid the study of defect location impact on the technique performance. A brief review of electromechanical impedance measurement and impedance-based NDE are first presented in this paper. Test specimens design and fabrication are then discussed in detail. Experimental results are then discussed and analyzed, followed by concluding remarks and future work directions.

IMPEDANCE-BASED NONDESTRUCTIVE EVALUATION

Impedance-based NDE is a vibration-based technique in nature. The fundamental basis of this technique is that the presence of manufacturing defects in the part under test alters the part's mass, stiffness, and damping characteristics, which in turn reflects on its dynamic response. Impedance-based NDE utilizes piezoelectric materials, lead zirconate titanate (PZT) wafers in particular, attached to the part under test as collocated sensors and actuators [7], [8]. Due to the coupled electromechanical behavior of piezoelectric materials, the electrical impedance of the piezoelectric transducer is related to the mechanical impedance of the part. Therefore, variations in the host structure due to printing defects are reflected on the easily measured electrical impedance of the piezoelectric transducers, which allows for such defects be detected and identified [9]–[11].

For most practical applications, thin piezoelectric wafer is bonded to a free surface of the part under test and is electrically excited through its thickness, as shown in Figure 1.a. For this configuration, the piezoelectric will be operating in the 31 mode. Assuming linear piezoelectricity, the constitutive equations of the piezoelectric materials can be expressed as follows [12]

$$\begin{aligned} \varepsilon_{11} &= s_{11}^{E}\sigma_{11} + d_{13}E_3 \\ D_3 &= (d^T)_{31}\sigma_{11} + \epsilon_{33}^{\sigma}E_3 \end{aligned} \tag{1}$$

where ε_{11} is the normal strain in the 1-direction, σ_{11} is the corresponding component of the work-conjugate stress tensor, D_3 is the electric displacement in the 3-direction, E_3 is the electric field in the 3-direction, d_{13} is the piezoelectric coupling coefficient, s_{11}^{E} is the complex mechanical compliance of the piezoelectric material measured at zero electric field, and ϵ_{33}^{σ} is the complex permittivity measured at zero stress.

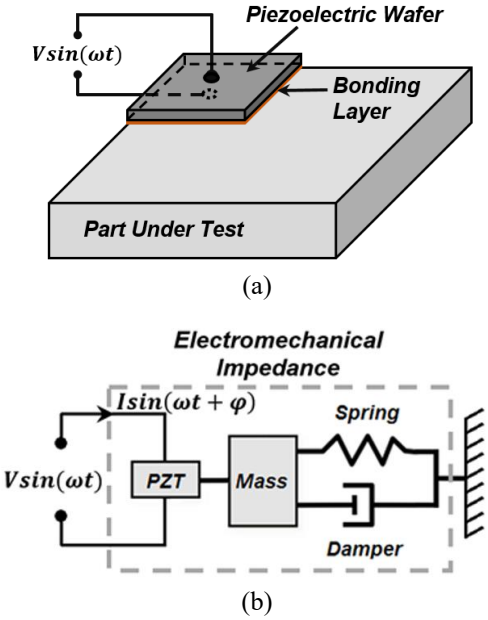

Figure 1. Impedance-based NDE (a) piezoelectric transducer attached to the part under test, and (b) schematic of the electromechanical impedance.

For a certain frequency range, the dynamic response of the part under test can be approximated as a single degree of freedom system, as shown in Figure 1.b. For this system, modal mass, stiffness, and damping are denoted by m_r, k_r, and ζ_r, respectively. Assuming perfect bonding between the piezoelectric wafer and the part under test, the electrical impedance of the piezoelectric transducer can be expressed as a function of the characteristics of the part under test, and those of the piezoelectric wafer, as follows [9]

$$Z(\omega) = \left[i\omega \frac{bl}{h}\left(\frac{d_{13}^2}{s_{11}^{E}}\left(\frac{tan(kl)}{kl}\left(\frac{Z_{pzt}}{Z_{pzt}+Z_{st}}\right)-1\right)+\bar{\epsilon}_{33}^{\sigma}\right)\right]^{-1} \tag{2}$$

where $Z_{pzt} = -iblh(s_{11}^{E}\omega\, tan(kl)/kl)^{-1}$ is the piezoelectric transducer short circuit impedance, $Z_{st} = 2\zeta_r(k_r m_r)^{1/2} + i(m_r\omega^2 - k_r)/\omega$ is the mechanical impedance of the part under test, $k = \omega(\rho \bar{s}_{11}^{E})^{1/2}$ is the wave number, ρ is the density of the piezoelectric material, b, h, $2l$ are the piezoelectric patch width, thickness and length, respectively.

As implied in equation 2, the sensitivity of impedance-based NDE to printing defects is dependent on the frequency range at which the part is interrogated. For small defects to be detected, higher modes of vibration need to be interrogated, and thus the part needs to be excited at high frequency. Besides the characteristic length of the defect to be detected, the optimal

frequency range is also dependent on the characteristics of the piezoelectric transducer itself [13].

In this study, impedance-based NDE is used with a supervised learning approach to detect the presence of build defects. This is the same approach used by the authors in a previous research effort [5]. With a supervised learning approach, the impedance signatures of the parts being tested are compared to a baseline signature from a known defect-free part. Thus, changes in a part's impedance signature compared to the baseline signature is used as an indicator of printing defects. In order to quantify the variations in the impedance signatures among different parts, damage metrics based on Root Mean Square Deviation (RMSD) and correlation coefficient (r) are calculated as follows:

$$RMSD = \sqrt{\sum \frac{(Z_D - Z_{BL})^2}{Z_{BL}^2}} \tag{3}$$

$$r = 1 - \left| \frac{n\sum Z_D Z_{BL} - \sum Z_D \sum Z_{BL}}{\sqrt{\left[n\sum Z_D^2 - (\sum Z_D)^2\right]\left[n\sum Z_{BL}^2 - (\sum Z_{BL})^2\right]}} \right| \tag{4}$$

where Z_D is the impedance signature of the part being tested, Z_{BL} is the baseline impedance signature, and n is the total number of data points in the impedance signature.

Following these definitions, the value of the damage metrics approaches zero when the two signatures are matching perfectly and increases as the response of the part under test starts to deviate from the baseline signature.

TEST SPECIMEN DESIGN AND FABRICATION

For this study, a set of test specimens has been designed in the form of rectangular beams to facilitate the investigation of internal voids effects on electromechanical impedance measurements. Each test specimen measures 72.5 x 7.25 x 5 mm, not including the 1 mm height of the L-shaped rails used to align the piezoelectric transducers, as shown in Figure 2. The placement of the transducers at the extreme end of each beam is chosen in order to avoid nodal lines in the bending vibration modes of the beam, and thereby increase the number of modes excited during impedance measurements.

The specimens are fabricated using a Fused Deposition Modeling (FDM) process, in which parts are built up by extruding a filament of model material through a heated nozzle. The process parameters used to fabricate the test specimens are detailed in Table 1. This process leads to two types of porosity in the fabricated parts:

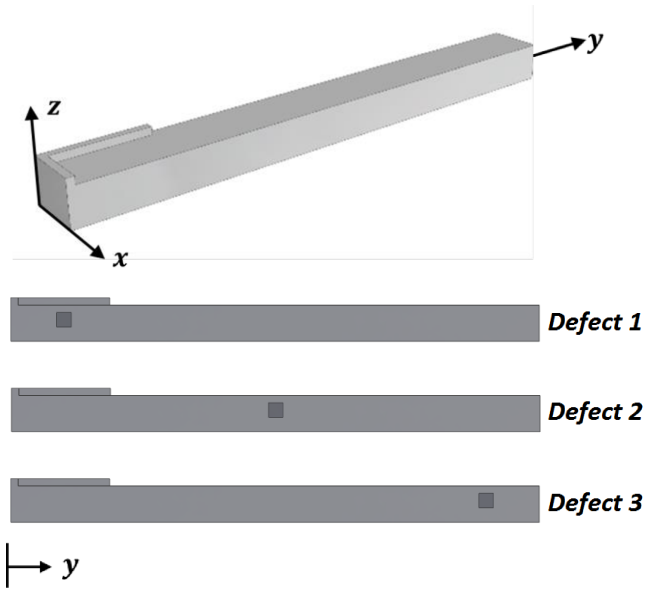

Figure 2. Test specimen schematics showing the overall shape and the three void locations tested.

I. Distributed internal porosity caused by the individual lines of extruded model material not completely flowing together to create a fully dense part
II. Local voids that are caused by an interruption in the flow through the nozzle.

While these effects are of interest, they are inherently difficult to study. The parameters that affect distributed internal porosity, such as infill pattern and filament feed rate, are not user-accessible on the machine used for fabrication. Furthermore, interruptions in nozzle flow are difficult to reproduce reliably unless they are several nozzle-widths in each dimension. Therefore, the defects investigated in this study have been designed to be large enough such that they can be reliably produced. Moreover, such defects are more consistent with a defect that might be introduced by a cyber-physical attack or a particularly bad clog at the nozzle.

In this study, two specimens in the test set are designed to be defect-free to establish a baseline signature, as discussed in the following sections. Defective parts, on the other hand, have been designed to have cubic voids with a side length of 2 mm. This defect size is chosen such that it is large enough to be consistently sized and sparsely-filled with support material in each specimen. Consistent sizing is considered important in order to isolate the effect of void placement on the measured response. Furthermore, filling the void with support material decreases mass differences among the parts. It is estimated that the void was approximately 50% dense with support material, based on the toolpath for the part. The density of the support material has not been reported by the manufacturer, however, it is measured to be approximately 120% of the density of the model material.

Table 1. Details of the machine, material, and process parameters used for test specimens fabrication.

Machine Model	Stratasys Fortus 450mc
Model Material	Stratasys Nylon 12
Support Material	Stratasys SR-110
Nozzle Temperature	355 °C
Build Chamber Temperature	120 °C
Layer Height	0.01” (0.254 mm)

Each of the three defective specimens has a void at one of three locations along its length: 7.3 mm, 36.25 mm, or 65.2 mm, as shown in Figure 2, which will be referred to as Defect 1, Defect 2, and Defect 3, respectively. These locations represent the midpoint of the piezoelectric transducer, the midpoint of the beam, and a point far away from the transducer. The voids are centered widthwise in the cross section, and located 1 mm below the surface on which the piezoelectric transducer is mounted.

After fabrication, the specimens were post-processed in an attempt to replicate what a typical part made using this machine would go through. After the parts were removed from the build tray, they were cleaned of support material by a soak in a basic solution. This cleaning was required in order to remove the raft of support material between the part and the build platform. The specimens were removed from the solution after two hours when no exterior support material was visible. All specimens were then rinsed and dried thoroughly before being left to air-dry for 24 hours.

EXPERIMENTAL SETUP

Once test specimens are printed, piezoelectric transducers are bonded to each of them guided by the L-shaped feature described in the previous section. Figure 3 shows the instrumented test specimens. All piezoelectric transducers are diced out of the same piezoelectric wafer and to the same dimensions (12.7mm × 6.35 mm) so as to minimize uncertainties introduced by piezoelectric patches characteristics. Glue is used to bond the piezoelectric patches to the test specimens.

For each test specimen, the impedance signature is measured using KEYSIGHT E4990A impedance analyzer. The frequency ranges selected for this study are 4-35 KHz. Beyond this frequency range impedance signatures of the defect-free control parts start to deviate, as discussed in the following sections. For all test specimens, the frequency sweep is performed with a 10 Hz resolution. The impedance analyzer excites the piezoelectric transducer with a one-volt peak-to-peak sinusoidal signal and allows the structure to settle before measuring its response. To minimize the effects of noise contamination, eight measurements were averaged at each frequency step. Figure 4 shows one of the test specimens connected to the impedance analyzer during impedance measurement. To compensate for the inconsistency in connectors’ resistivity, as a result of soldering variations, all impedance signatures are shifted vertically such that their average value, excluding impedance peaks, match over the frequency range of interest.

Figure 3. Test specimens instrumented with piezoelectric transducers.

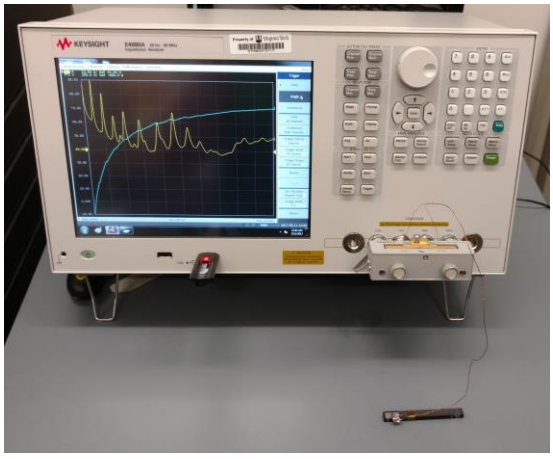

Figure 4. KEYSIGHT E4990A impedance analyzer measuring the impedance signature of one specimen.

RESULTS AND DISCUSSION

In this section, the impedance signatures of all test specimens are presented and analyzed. The baseline is first calculated based on the control parts signatures. Results from defective parts (with internal voids) are then presented and compared to the baseline signature.

BASELINE MEASUREMENT

A baseline signature is first established by measuring and averaging the electromechanical impedance signatures of the two defect-free control parts. Figure 5 shows the real component of the impedance signatures of each control part along with the averaged response for the 5-97 kHz frequency range. As suggested by the figure, impedance signature of the two control parts are in very good agreement at low-frequency ranges and they start to deviate at higher frequencies.

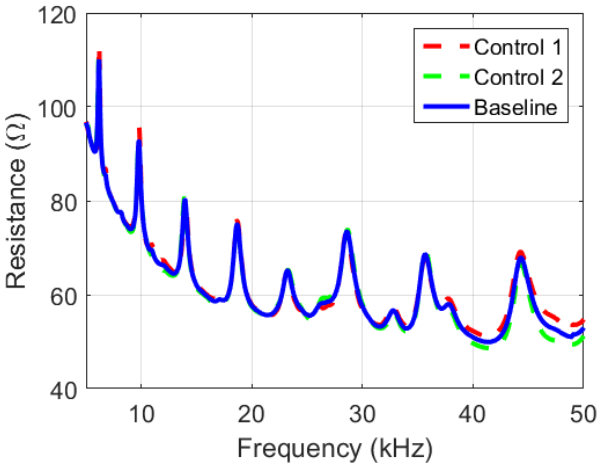

(a)

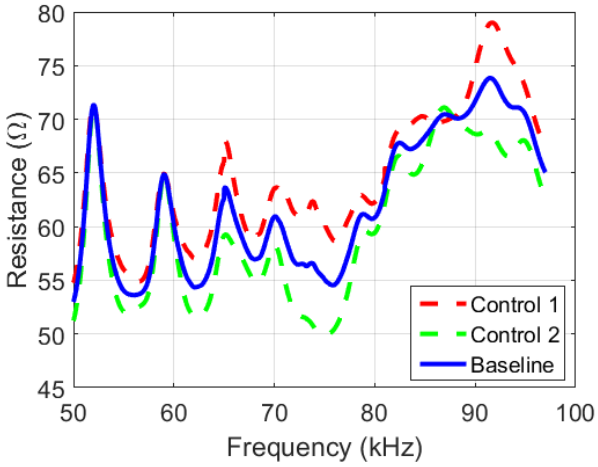

(b)

Figure 5. Real component of the impedance signatures for the defect-free (control) parts along with the baseline signature for (a) 5 kHz - 50 kHz, and (b) 50 kHz - 97 kHz frequency range.

This deviation can be ascribed to imperfections associated with piezoelectric transducers bonding process, manufacturing tolerances, or unknown defects in the assumed defect-free parts. In-depth uncertainty analysis will be conducted in future studies to quantify the contribution of the aforementioned factors.

In order to quantify the discrepancies between the control parts and the averaged baseline signature, damage metrics are calculated. The frequency range is first split into 24 sub-bands, 4 kHz each, and the RMSD and Correlation Coefficients damage metrics are calculated for each sub-band. The results are shown in Figure 6 for Control 2. It is found that up to 40 kHz, control parts are in very good agreement. Beyond this frequency, larger values of damage metrics are obtained for the control parts, which indicates less confidence in the defect-free response. Therefore, the frequency range used for impedance-based NDE in this study is limited to 40 kHz.

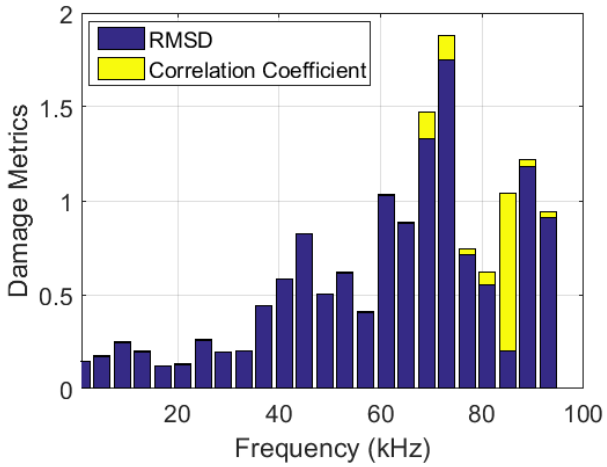

Figure 6. Damage metrics values for Control 2 as compared to the Baseline.

EFFECTS OF INTERNAL POROSITY

To investigate the sensitivity of impedance-based NDE to internal porosity defects, three test specimens featuring this build defect are investigated. All three specimens have the same void size (2×2×2 mm^3), but they are at different locations along the beam as discussed in the "*Test Specimen Design and Fabrication*" section. Impedance signatures for all specimens are measured over the frequency range of 1-97 kHz, however, the analysis is limited to the 5-40 kHz range, as discussed in the previous section. Figure 7 shows the impedance signature of each defective part as compared to baseline signature.

In general, the impedance signatures of defective parts are close to the baseline signature, except for vertical shifts, which can be a result of variations in connector's resistivity. Frequency shifts of impedance peaks are also noticed. For instance, the peak originally located at 28.58 kHz was found to shift to 28.34 kHz upon the introduction of Defect 2. This reduction in impedance peak frequency indicates that the effect of stiffness loss (due to the presence of internal voids) on the dynamic response of the part is more dominant than the accompanying mass loss.

The sharp peaks in the impedance signatures corresponding to Defect 1 and Defect 2 suggest a reduction in damping of these parts, unlike Defect 3 which appears to have larger damping compared to the defect-free parts. This could be ascribed to the voids being filled, or not filled, with the support material. Further investigations are required to explain these changes.

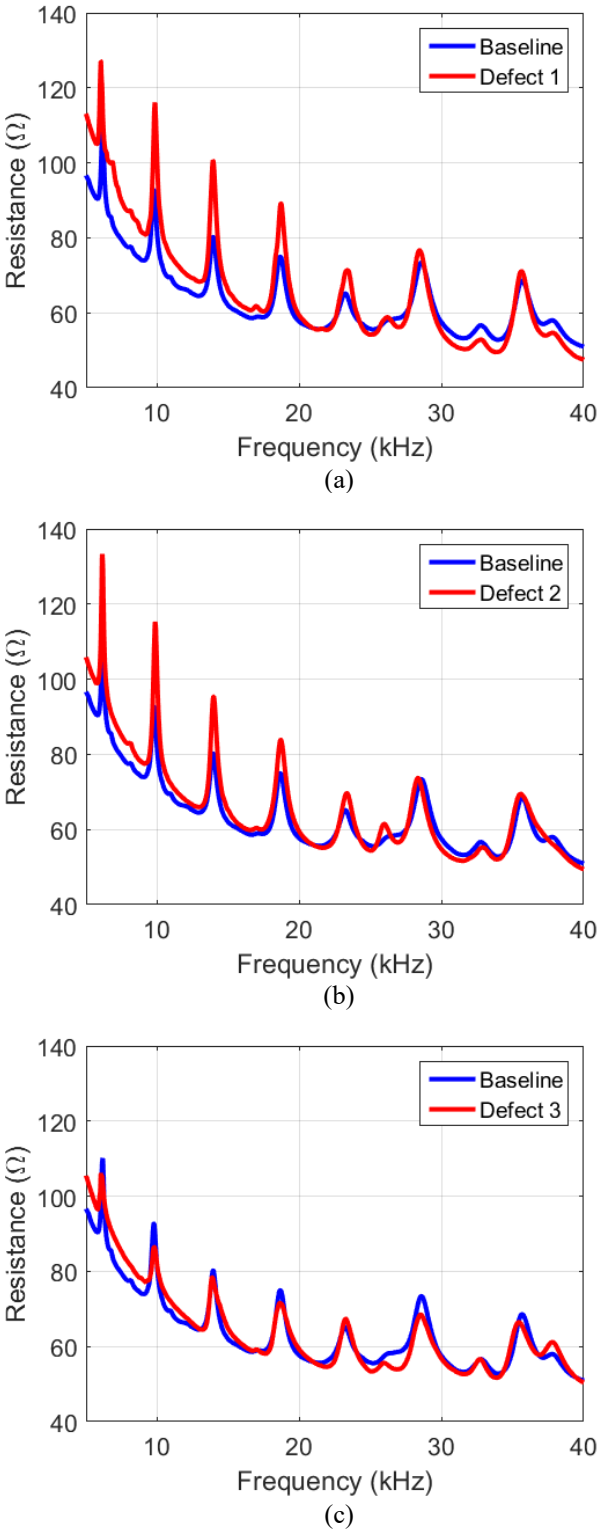

Figure 7. Impedance signatures of the defective parts as compared to the baseline signature. (a) Defect 1, (b) Defect 2, and (c) Defect 3.

Figure 8 shows the damage metrics, both RMSD and correlation coefficient, for the three defective parts. It can be noticed that the internal void defects can be clearly detected with impedance-based NDE. Although the values of the correlation coefficient damage metric for the defective part are very small, they are an order of magnitude larger than those corresponding to the control part. RMSD damage metric, on the other hand, tends to overestimate the effects of internal voids due to the vertical shift in the impedance signature. The sensitivity of impedance-based NDE is expected to further enhance if the parts are interrogated at higher frequencies. However, utilizing such high frequencies require addressing the different sources of uncertainty discussed in the "*Baseline Measurement*" section.

Finally, no clear trends have been noticed regarding the effects of voids location on the sensitivity of impedance-based NDE. Further analysis is required to correlate the effect of defect location on the measured impedance signature. Model-based techniques coupled with machine learning algorithms can be utilized for this purpose. This will be addressed by the authors in future studies.

CONCLUSIONS

In this work, the effectiveness of impedance-based NDE approach to detect internal porosity in AM parts is investigated. A suite of test specimens, in the form of simple rectangular beams, has been designed featuring this build error. Voids are introduced to the parts at several locations (right underneath the piezoelectric transducer, in the middle of the beam, and towards the far end) to study the effect of defect location on the technique's performance.

Consistent impedance signatures for the defect-free parts has been obtained up to 40 kHz. Beyond this frequency, the responses of the control parts started to deviate. This deviation can be ascribed to a number of factors including piezoelectric transducers bonding imperfections, manufacturing tolerances, or unknown defects in the control parts. Further investigations will be conducted to quantify the contribution of these factors to uncertainty in the baseline measurement. By analyzing the electromechanical impedance signatures of the defective parts, internal porosity build errors (in the form of 2×2×2 mm^3 voids) have been successfully detected. Upon calculating damage metrics, it was found that RMSD definition tends to overestimate the effects of internal voids. This is due to the vertical shift in the impedance signature, which includes the effects of variations in connectors' resistivity.

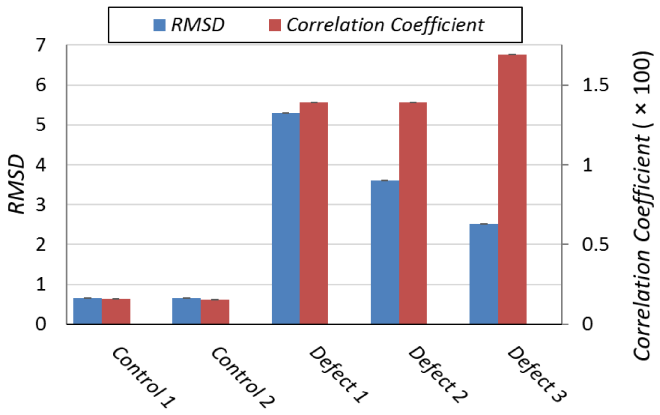

Figure 8. Damage metrics for void defects.

Close examination of impedance signature shows that the introduction of voids causes impedance peaks to shift to lower frequencies. This is a direct result of stiffness reduction of the beam associated with the presence of internal voids. While abstract damage metrics fail to reveal clear trends regarding defect location, in-depth analysis of impedance signatures (coupled with numerical models or machine learning algorithms) provide more insight regarding defects location and severity.

ACKNOWLEDGMENT

This material is based upon work supported by the National Science Foundation under Grant Number 1635356. Any opinions, findings, and conclusions or recommendations expressed in this material are those of the authors and do not necessarily reflect the views of the National Science Foundation.

REFERENCES

[1] J. M. Waller, B. H. Parker, K. L. Hodges, E. R. Burke, and J. L. Walker, "Nondestructive Evaluation of Additive Manufacturing State-of-the-Discipline Report," Nov. 2014.

[2] A. du Plessis, S. G. le Roux, J. Els, G. Booysen, and D. C. Blaine, "Application of microCT to the non-destructive testing of an additive manufactured titanium component," *Case Stud. Nondestruct. Test. Eval.*, vol. 4, pp. 1–7, 2015.

[3] M. I. Albakri, L. Sturm, C. B. Williams, and P. A. Tarazaga, "Non-destructive evaluation of additively manufactured parts via impedance-based monitoring," presented at the International Solid Freeform Fabrication Symposium, Austin, TX., August, 2015.

[4] L. Sturm, M. I. Albakri, P. A. Tarazaga, and C. B. Williams, "In-situ Detection of Build Defects in Additive Manufacturing via Impedance-Based Monitoring," presented at the International Solid Freeform Fabrication Symposium, Austin, TX., August, 2016.

[5] M. I. Albakri, L. Sturm, C. B. Williams, and P. A. Tarazaga, "Impedance-based non-destructive evaluation of additively manufactured parts," *Rapid Prototyp. J.*, Vol. 23 Issue: 3, pp.589-601, 2017.

[6] L. D. Sturm, C. B. Williams, J. A. Camelio, J. White, and R. Parker, "Cyber-physical vulnerabilities in additive manufacturing systems: A case study attack on the .STL file with human subjects," *J. Manuf. Syst.*, vol. 44, Part 1, pp. 154–164, 2017.

[7] C. Liang, F. P. Sun, and C. A. Rogers, "Coupled Electro-Mechanical Analysis of Adaptive Material Systems — Determination of the Actuator Power Consumption and System Energy Transfer," *J. Intell. Mater. Syst. Struct.*, vol. 5, no. 1, pp. 12–20, 1994.

[8] M. I. Albakri and P. A. Tarazaga, "Dynamic analysis of a piezoelectric augmented beam system with adhesive bonding layer effects," *J. Intell. Mater. Syst. Struct.*, vol. 28, no. 2, pp. 178–194, 2017.

[9] G. Park, H. Sohn, C. R. Farrar, and D. J. Inman, "Overview of piezoelectric impedance-based health monitoring and path forward," *Shock Vib. Dig.*, vol. 35, no. 6, pp. 451–463, 2003.

[10] G. Park, H. H. Cudney, and D. J. Inman, "An Integrated Health Monitoring Technique Using Structural Impedance Sensors," *J. Intell. Mater. Syst. Struct.*, vol. 11, no. 6, pp. 448–455, 2000.

[11] M. I. Albakri and P. A. Tarazaga, "Electromechanical impedance–based damage characterization using spectral element method," *J. Intell. Mater. Syst. Struct.*, vol. 28, no. 1, pp. 63–77, 2017.

[12] D. J. Leo, *Introduction to Smart Material Systems*. John Wiley & Sons, Inc., 2007.

[13] D. M. Peairs, P. A. Tarazaga, and D. J. Inman, "Frequency Range Selection for Impedance-Based Structural Health Monitoring," *J. Vib. Acoust.*, vol. 129, no. 6, pp. 701–709, 2007.